2009

Remote Measurements Of Thundercloud Electrostatic Fields

Joseph R. Dwyer

Martin A. Uman

Hamid K. Rassoul

Remote measurements of thundercloud electrostatic fields

J. R. Dwyer,[1] M. A. Uman,[2] and H. K. Rassoul[1]

Received 30 October 2008; revised 17 February 2009; accepted 6 March 2009; published 7 May 2009.

[1] Analytical and numerical models of the radio frequency emissions produced by relativistic runaway electron avalanches initiated by cosmic ray extensive air showers are presented. It is found that single-point measurements of the distant electromagnetic fields allow the remote determination of the electrostatic field in the runaway electron avalanche region. For instance, it is possible to use ground-based and/or remote airborne measurements of the radio frequency pulses from the runaway electron avalanches to map the magnitudes and directions of the electrostatic field within a thundercloud for regions with electric fields above the runaway avalanche threshold. Such measurements, which are difficult to perform in situ, may help answer several key questions regarding lightning initiation, such as what electric fields are usually present when lightning initiates and whether electric fields in small regions ever reach the conventional breakdown field.

Citation: Dwyer, J. R., M. A. Uman, and H. K. Rassoul (2009), Remote measurements of thundercloud electrostatic fields, *J. Geophys. Res.*, *114*, D09208, doi:10.1029/2008JD011386.

1. Introduction

[2] One of the major uncertainties hindering progress in understanding thundercloud electrification and lightning initiation is that the range of the electric fields inside thunderclouds is not known [e.g., *Rakov and Uman*, 2003, pp. 82–84]. In particular, the maximum value of the electric field, which is likely related to lightning initiation, is unknown. Further, it is not known over what spatial extent and for what time the largest fields persist.

[3] Measurements in situ by balloons, aircraft, and rockets have found that the maximum electric field inside thunderclouds, scaled to the equivalent field at sea level, rarely exceeds about 4.0×10^5 V/m, about one third the value required to initiate a conventional discharge, even when the effects of precipitation are included [*MacGorman and Rust*, 1998; *Solomon et al.*, 2001]. This has led many researchers to speculate that if the electric fields do reach the level required for conventional breakdown, they do so in either localized regions or over very short time periods that are not likely to be observed with in situ measurements.

[4] As an alternative to conventional breakdown, it has been suggested that runaway electrons play some role in lightning initiation [*Gurevich et al.*, 1999; *Gurevich and Zybin*, 2001]. Runaway electrons are produced when the rate of energy gain by electrons moving through an electric field exceeds the rate of energy loss produced mainly by ionization of the air [*Gurevich et al.*, 1992]. Such runaway electrons produce other runaway electrons through an avalanche process, resulting in an exponentially growing population of energetic multi-MeV electrons. This association of runaway electrons with lightning initiation has been motivated by the fact that the maximum observed thundercloud field is often near or slightly above the runaway electron avalanche threshold field E_{th} = 284 kV/m (n/n_o), where n and n_o are the densities of air at the altitude under consideration and at sea level for standard conditions, respectively [*Marshall et al.*, 2005; *Dwyer*, 2003]. Although runaway electron avalanches can occur for electric field strengths about one order of magnitude lower than for conventional breakdown, in order to produce significant ionization, the region with $E > E_{th}$ must extend over large distances (e.g., many tens of meters to kilometers, depending upon the electric field), thus requiring relatively large potential differences, on the order of hundreds of millions of volts. Directly observing such fields may be very difficult because the fields may only remain large for times much shorter than is required to traverse the region with balloons or aircraft [*Dwyer*, 2005].

[5] The difficulty in measuring the thundercloud electric fields in situ has hampered progress in understanding the mechanism(s) involved in initiating lightning and in constraining thunderstorm electrification models. The experimental challenge of directly measuring electric fields inside thunderclouds has been daunting. The active regions of thunderclouds can cover many cubic kilometers, with violent weather conditions, making it difficult to operate balloons and dangerous to operate manned aircraft. Furthermore, in situ measurements give just snap shots of the electric field at a few locations, making it challenging to piece together the observations to gain an accurate picture of the large-scale electric fields.

[6] In this study, a new technique is introduced for making remote (e.g., ground based or airborne) measurements of the static or slowly varying electric fields inside thunderclouds. This technique involves measurements of the radio frequency electromagnetic fields emitted by cosmic ray extensive air showers (EASs) that traverse regions with

[1]Department of Physics and Space Sciences, Florida Institute of Technology, Melbourne, Florida, USA.
[2]Department of Electrical and Computer Engineering, University of Florida, Gainesville, Florida, USA.

0148-0227/09/2008JD011386

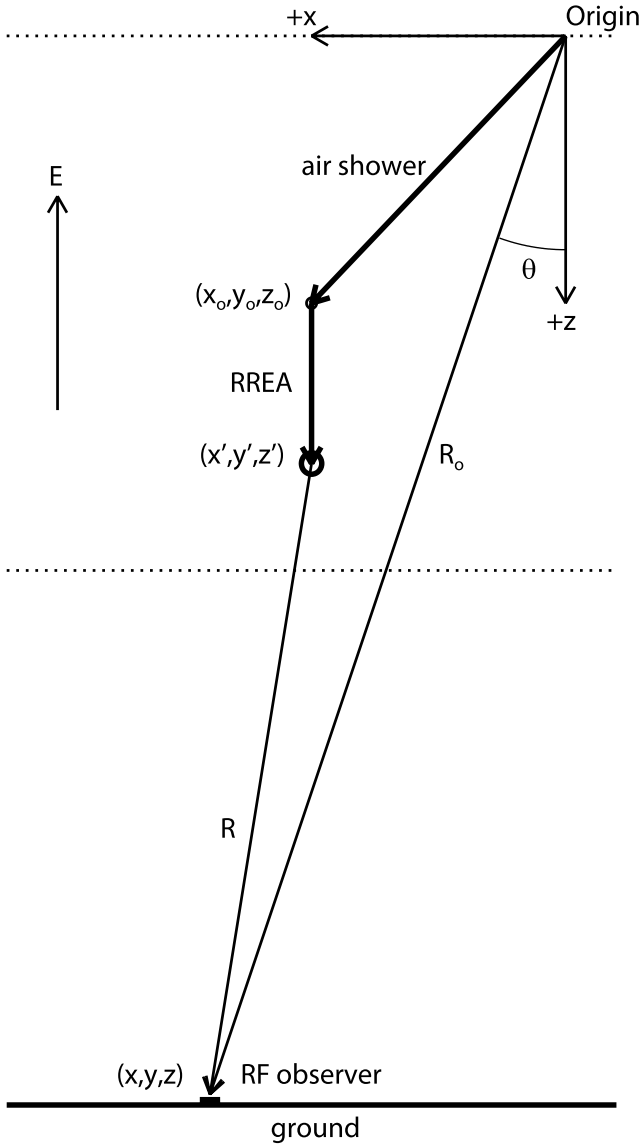

Figure 1. Diagram showing the coordinate system used in this study for the case of an upward electric field.

$E > E_{th}$. Specifically, in this study, both analytical and numerical models of the electromagnetic fields produced by runaway electron avalanches will be developed. The results of these models will be used to demonstrate that the electrostatic or slowly varying field at the source (e.g., inside the thundercloud) can be obtained by remote measurements of either the electric or magnetic field waveforms of radio frequency pulses. For example, a single electric field antenna, colocated with a modest air shower array should be able to map the electric field magnitude and polarity as a function of the position and time within thunderclouds in the vicinity.

2. Model Overview

2.1. Runaway Electron Physics

[7] When atmospheric cosmic ray particles (e.g., electrons, positrons, and muons) impinge upon a region in which the electric field strength is greater than the runaway electron avalanche threshold, the cosmic rays will serve as seeds for relativistic runaway electron avalanches (RREAs). As noted earlier, runaway electrons occur when the electric force exceeds the effective frictional force experienced by electrons in air. As the runaway electrons interact with air, they will produce energetic "knock-on" electrons that can also runaway. The result is an avalanche of relativistic electrons that increases exponentially with distance and time, with an average energy of 7.3 MeV, independent of the electric field strength and the air density [*Dwyer*, 2004; *Coleman and Dwyer*, 2006]. Such energetic electrons produce copious numbers of X-rays via bremsstrahlung interactions with air, plus large amounts of ionization.

[8] Several previous authors have calculated the radio frequency (RF) emission from cosmic ray extensive air showers and runaway electron avalanches (sometimes referred to as runaway breakdown), with a range of different results [*Roussel-Dupré and Gurevich*, 1996; *Gurevich et al.*, 2002, 2004a, 2006; *Gurevich and Zybin*, 2004; *Tierney et al.*, 2005]. Here we shall provide a new detailed derivation of the RF emission starting from established properties of cosmic ray extensive air showers (hereafter referred to simply as air showers) and runaway electron avalanches. A comparison with earlier work will be presented in section 3.2.

[9] In addition, there exists considerable literature regarding radio emission from cosmic ray air showers not involving runaway electron avalanche multiplication [e.g., *Jelley et al.*, 1965; *Tompkins*, 1974; *Buitink et al.*, 2007]. Most of this work involves synchrotron emission of electrons and positrons in the shower moving in the geomagnetic field [*Kahn and Lerche*, 1966]. However, this geosynchrotron emission from the air showers is usually quite small (e.g., usually measured in μV m^{-1} MHz^{-1}) and is highly beamed in the direction of the shower, with the electric field strength decreasing exponentially with an e-folding distance of about 100 m from the shower center [*Huege and Falcke*, 2005]. The RF emission discussed in this study, which results from the current due to avalanche multiplication of runaway electrons, should be distinguishable from such geosynchrotron emission.

[10] The basic geometry used in this study is shown in Figures 1 and 2. Figure 1 is for the case of an upward pointing electric field, e.g., corresponding to the field below the main negative charge center inside a thundercloud. Figure 2 is for the case of a downward pointing electric field, e.g., corresponding to the field between the main negative and main positive charge centers. In the figures, the dotted lines indicate the regions with high electric fields above the runaway electron avalanche threshold. Relativistic runaway electron avalanches (labeled RREA) propagate in the opposite direction of the electric field vectors. The coordinate system is defined such that the cosmic ray air showers, which provides seed particles for the runaway electron avalanches, always travel in the $+x$ direction and passes through the origin. The $+z$ direction is always chosen to point in the same direction that the runaway electrons propagate and with $z = 0$ coinciding with the location that the air shower crosses the start of the avalanche region, regardless of the actual direction that the electric field points with respect to the ground. In this study, the location and time of the air shower are labeled (x_o, y_o, z_o, t_o) and the location and time of the avalanche, seeded by the air shower, are labeled (x', y', z', t'). Finally, the location

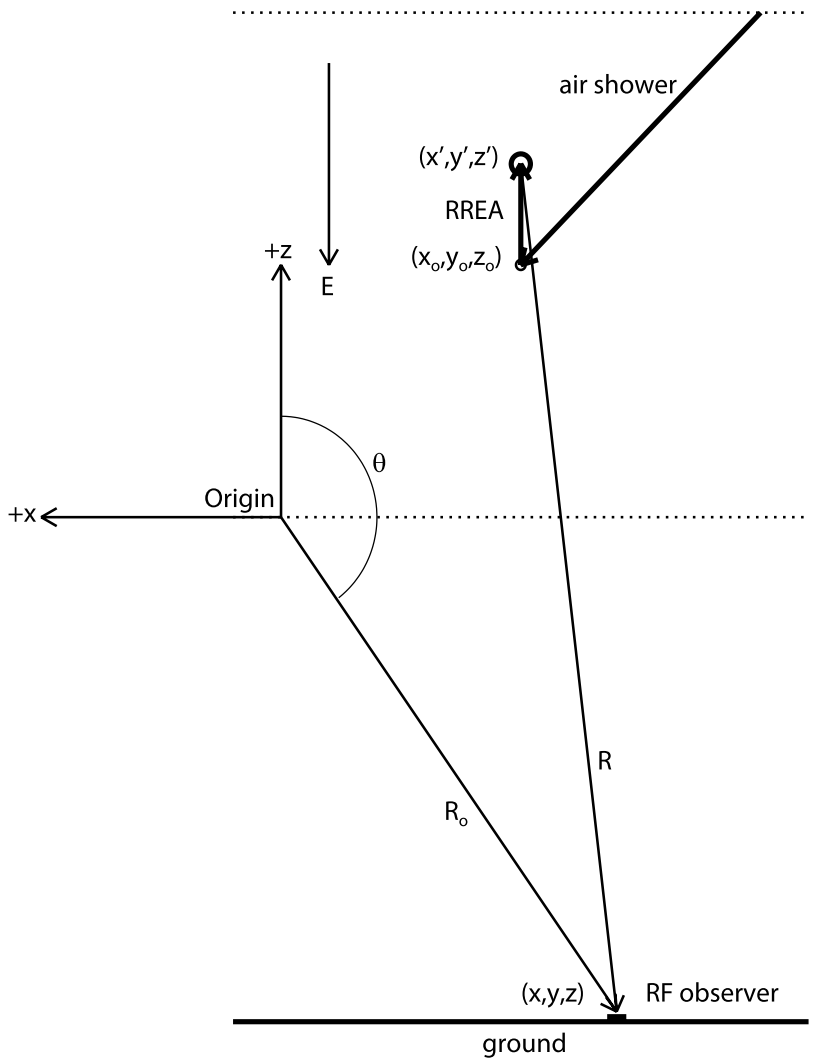

Figure 2. Diagram showing the coordinate system used in this study for the case of a downward electric field.

and time of the RF observer are labeled (x, y, z, t). The vector labeled R_o in the figures points in the direction of the unit vector, $\hat{n}$, which has the angle θ with respect to the $+z$ axis as shown. The vector labeled R is the vector connecting the RF source to the RF observer. In the analytical model presented below, it will be assumed that R and R_o are large enough compared to the size of the avalanche region that R also has the same angle θ with respect to the $+z$ axis.

[11] Although the average kinetic energy of runaway electrons in an avalanche is 7.3 MeV, the propagation speed of the center of the avalanche is only about $0.89c$ [*Coleman and Dwyer*, 2006]. It then follows that the runaway electron avalanche moves with an average velocity $\vec{v}_{re} = 0.89c\hat{z}$. The cosmic ray air shower velocity will be denoted, $\vec{u}$, and will have a speed very close to the speed of light, c.

[12] A slightly more realistic diagram is shown in Figure 3 for an upward electric field. In Figure 3, the cosmic ray extensive air shower (blue dots labeled EAS) propagates downward (toward the earth) and to the left at an incident angle, θ_{cr}. In the Figure, as the air shower particles enter the avalanche region labeled, $E > E_{th}$, with a vertical electric field, they produce runaway electrons that then propagate downward generating a relativistic runaway electron avalanche, black dots labeled runaway electrons. The low-energy electrons that are produced by ionization (red dots labeled slow electrons) drift downward before attaching, forming a distribution that follows behind the runaway electrons.

[13] Although the charge associated with the runaway and low-energy electrons moves with constant velocity, its magnitude and hence the current increases exponentially with time during the avalanche multiplication, resulting in the emission of electromagnetic radiation in the radio frequency (MHz) range. As in Figures 1 and 2, the observer (i.e., antenna) that records the radio frequency pulse is located at angle θ with respect to the avalanche (runaway electron) direction. At the end of the avalanche region, where $E < E_{th}$, the number of runaway electrons will decrease with distance, causing the current to decrease, causing the RF pulse to become bipolar.

[14] The low-energy positive and negative ions that result from the ionization of the air by the runaway electrons and the subsequent attachment of the low-energy electrons do not contribute significantly to the current density because of

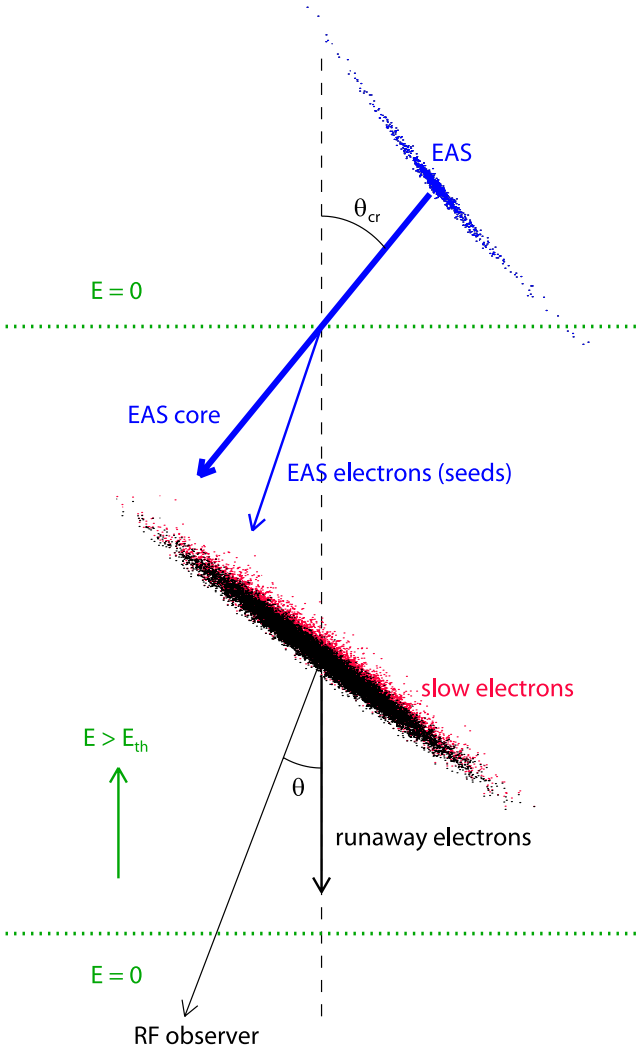

Figure 3. Schematic diagram showing an extensive air shower (blue dots labeled EAS) entering a high electric field region, wherein runaway electron avalanches are produced (black dots). The electric field points upward. The low-energy electrons (red dots labeled slow electrons) resulting from ionization by the runaway electrons trail behind the runaway electrons. As the air shower passes through the high-field region, the muons and hadronic core are not significantly deflected by the electric force, and so the location that the air shower strikes the ground is unchanged. However, the electric field locally causes large deflections of the electrons (and positrons) in the shower, which make the largest contribution to the runaway electron seed population. For the case of a downward electric field, the air shower still enters through the top of the avalanche region, as shown, and propagates to the bottom of the region. However, the runaway electrons and the low-energy electrons all propagate upward in this case. As the runaway avalanches propagate and grow, the increasing electric current produces RF emission that can be measured remotely.

their very low drift speeds. The ions, however, do make an important contribution to the total charge density. However, as will be discussed below, only the current density produced by the runaway electrons and low-energy (drifting) electrons is required in order to calculate the electromagnetic RF fields. Therefore the low-energy ions need not be directly considered in these calculations.

[15] At the simplest level, the avalanche multiplication factor of the runaway electrons, N_{re}, is described by

$$dN_{re} = N_{re}\frac{dz}{\lambda}, \tag{1}$$

where λ is the avalanche (e-folding) length. The avalanche length, which depends upon the local electric field strength and the air density, is given over the range 3.0×10^5 V/m $(n/n_o) < E < 3.0 \times 10^6$ V/m (n/n_o) by the empirical expression

$$\lambda = \frac{7.3 \times 10^6\ \mathrm{V}}{(E - E_o)}, \tag{2}$$

determined from fits to Monte Carlo simulation results [*Dwyer*, 2003; *Coleman and Dwyer*, 2006], where λ has units of meters and E has units of V/m. The parameter

$$E_o = 2.76 \times 10^5\ \mathrm{V/m}(n/n_o) \tag{3}$$

is approximately equal to the runaway avalanche threshold field $E_{th} = 2.84 \times 10^5$ V/m (n/n_o). For electric field strengths below the runaway avalanche threshold, the number of runaway electrons exponentially decays with distance. Monte Carlo simulations show that in this case equations (1) and (2) remain approximately true with $E_o \approx 3.2 \times 10^5$ V/m (n/n_o). In this case, λ is negative and the number of runaway electrons exponentially decays.

[16] For the conditions under consideration in this study, we may safely ignore the effects of the self-generated electromagnetic fields on the runaway electron avalanche development and the low-energy electron propagation. Specifically, because the avalanche multiplication factor is always less than 10^5, consistent with the limits set by relativistic feedback [*Dwyer*, 2007, 2008], the currents and charge transfer produced by the runaway electron avalanche and the accompanying low-energy electrons produce an insignificant electromagnetic field perturbation compared with the ambient electric field that is driving the avalanche.

[17] For an avalanche starting at position z_o and measured at position z', equation (1) can be integrated directly to give

$$\begin{aligned} N_{re}(z', z_o) &= \exp\left(\int_{z_o}^{z'} \frac{dz''}{\lambda}\right) S(z_o) S(L - z') S(z' - z_o) \\ &= \exp(\xi(z', z_o)) S(z_o) S(L - z') S(z' - z_o), \end{aligned} \tag{4}$$

where ξ is the number of avalanche (e-folding) lengths. For convenience, the start of the avalanche region is defined to be at $z = 0$ and the end of the avalanche region is defined to be at $z = L$. Throughout this study, the direction of runaway electron avalanche propagation will be defined to be the $+z$ direction, regardless of the electric field orientation inside the thundercloud. For example, this avalanche propagation direction will be downward if the electric field is vertical (upward).

[18] The step function, S, guarantees that only locations within the avalanche region ($0 < z < L$) are considered and that the avalanche propagates in the correct direction, opposite the electric field vector. The step function, $S(x)$ is defined to be equal to 0 for $x < 0$ and equal to 1 for $x \geq 0$. For the analytical model, developed in this study, we shall treat the electric field in the avalanche region as constant. In this case, equation (4) simplifies to

$$N_{re}(z', z_o) = \exp\left(\frac{(z' - z_o)}{\lambda}\right) S(z_o) S(L - z') S(z' - z_o). \quad (5)$$

Cases in which the electric field in the avalanche region vary with position will be treated using a numerical model in sections 4 and 5.

[19] In addition to avalanche multiplication, as the runaway electrons propagate, they undergo diffusion in both the lateral (x and y) and longitudinal (z) directions, due primarily to elastic scattering and velocity dispersion. For instance, detailed Monte Carlo simulations of runaway electron avalanches show that the RMS spread of the runaway electrons in the longitudinal direction is approximately $\lambda/3$ at the end of 10 avalanche lengths for a wide range of electric field strengths. In addition, for a 0.75 MV/m electric field at 5 km altitude, Monte Carlo simulations show that the RMS spread in the lateral direction (e.g., along the x axis) due to runaway electron scattering is about 14 m at the end of 10 avalanche lengths.

[20] Including avalanche multiplication and diffusion for a uniform electric field, for each energetic seed particle injected at the point (x_0, y_0, z_0, t_0), the number density of the runaway electrons in the avalanche is given approximately by

$$G_{re}(x', y', z', t'; x_o, y_o, z_o, t_o) = \frac{1}{(4\pi(t' - t_o))^{3/2} D_r D_z^{1/2}} \times \exp\left(\frac{v_{re}(t' - t_o)}{\lambda} - \frac{(x' - x_o)^2 + (y' - y_o)^2}{4D_r(t' - t_o)} - \frac{(v_{re}(t' - t_o) - (z' - z_o))^2}{4D_z(t' - t_o)}\right) S(t' - t_o) S(z_o) S(L - z'), \quad (6)$$

where D_z and D_r are the longitudinal and lateral diffusion coefficients. The longitudinal distribution (along the propagation direction) of the runaway electrons means that some runaway electrons will exit the avalanche region while others are still experiencing avalanche multiplication. As will be shown, this will reduce the amplitude of the resulting RF pulse. The lateral spread of the runaway electrons will also cause a spreading of the RF pulse due to the dispersion in arrival times of the RF signal, due to the differences in traveltime from one side of the avalanche to the other. This spreading, the effects of which are made more significant by the relativistic effects at small viewing angles, will be investigated in section 4.

[21] In the limit where D_r and D_z go to 0, equation (6) becomes

$$G_{re}(x', y', z', t'; x_o, y_o, z_o, t_o) = \exp((z' - z_o)/\lambda) \delta(v_{re}(t' - t_o) - (z' - z_o)) \cdot \delta(x' - x_o) \delta(y' - y_o) S(t' - t_o) S(z_o) S(L - z'), \quad (7)$$

where δ is the Dirac-delta function. equation (7) will be used in the analytical model presented in section 3. Multiplying equation (7) by the v_{re} gives the flux of runaway electrons. Integrating this flux over all x', y' and t' then gives back equation (5), the multiplication factor at position z'. More generally, for an arbitrary density of energetic seed particles, the charge density of runaway electrons is given by

$$\rho_{re}(x', y', z', t') = -e \iiint G_{re}(x', y', z', t'; x_o, y_o, z_o, t_o) \cdot n_s(x_o, y_o, z_o, t_o) dx_o dy_o dz_o dt_o, \quad (8)$$

where the function $n_s(x_o, y_o, z_o, t_o)$ is the density of energetic seed electrons that runaway injected per second.

2.2. Cosmic Ray Extensive Air Showers

[22] We now consider the effects of air showers traversing the runaway electron avalanche region. Extensive air shower are composed of three basic components: the nuclear active component, made up of very high-energy particles close to the shower axis: the muon component, which forms a broad lateral distribution, and the electronic component made up of electrons, positrons, and gamma rays. The electrons and positrons in the air shower are the result of electromagnetic cascades continuously generated by high-energy gamma rays from pion decays. At thunderstorm altitudes, the air shower is often near its maximum development. Near shower maximum, most of the particles in the shower are part of the electronic component. As the air shower propagates through a high-field region, due to their high rigidity, the nuclear and muon components are not significantly affected by the thundercloud electric fields. On the other hand, the electronic component can be substantially altered by the electric field, with electrons deflected in one direction and positrons in the other, depending upon the electric field direction. The propagation lengths of the electrons and positrons are also greatly extended (due to runaway), causing an increase in the total number of air shower particles over the case of no electric field. Indeed, the development of the electromagnetic cascades cannot be completely separated from the runaway electron production.

[23] At the top of the avalanche region, the number of secondary energetic particles at shower maximum that serve as seed particles for the runaway electron avalanche is described by the approximate relation

$$N_{EAS} \sim 5 \times 10^{-2} \mathcal{E}_{CR}^{1.1}, \quad (9)$$

where $\mathcal{E}_{CR}$ is the total energy of the cosmic ray primary measured in GeV [*Gaisser*, 1990, p. 240]. For example, N_{EAS} is $\sim 3 \times 10^7$ for a primary energy of 10^{17} eV.

[24] Monte Carlo simulations [see *Dwyer*, 2007] of the electromagnetic cascade, show that for electric fields above E_{th}, the particles (electrons or positrons) that runaway in the opposite direction of the air shower, diminish rapidly with distance. The other particles (electrons or positrons) that runaway in the same direction as the air shower grow approximately linearly with distance with a rate of change of about 10^{-2} m^{-1} $N_{EAS} \times (n/n_o)$. However, for the first

avalanche length from the top of the avalanche region, these effects roughly cancel, and the number of air shower particles in the first avalanche length is roughly constant. As a result, for upward electric fields, since the runaway electron avalanche develops rapidly after the first avalanche length, the number of seed particles can be approximated as constant throughout the avalanche region. Conversely, for downward electric fields, most of the runaway electrons result from seed particles near the bottom of the avalanche region, so the change in the air shower within the avalanche region is often substantial. In addition, it is found that the part of the electron and positron component that runs away in the downward direction is deflected toward the field line with an average propagation angle with respect to the field line about one half that of the shower core. This deflection is included in the analytical and numerical models.

[25] Because of the Lorentz contraction of the shower, the longitudinal thickness is highly compressed compared with the lateral size, and so the particles in an air shower form a thin layer, sometimes described as a thin pancake. At any one location on the shower front, the typical thickness is on the order of $\sim$1 m. However, the shower front has a slight curvature, on the order of a few hundred meters, resulting in an effective longitudinal thickness (deviation from a plane perpendicular to the shower axis) of roughly 10 m, with an approximately exponential falloff behind the front. The lateral distribution, perpendicular to the shower axis, is given by the well known NKG formula

$$(r/r_1)f(r/r_1) \propto (r/r_1)^{s-1}(1+r/r_1)^{s-4.5}, \tag{10}$$

where $1.0 \leq s \leq 1.4$ ($s = 1.0$ is used in this study) and r is the lateral (cylindrical) radius in units of g/cm^2 from the shower core [*Gaisser*, 1990, p. 226]. The constant $r_1 \sim 9.3$ g/cm^2 is the Moliere unit, characterizing the lower energy particles of the shower.

[26] For the analytical model, the lateral width and longitudinal thickness of the shower as well as the alteration of the shower by the electric field (other than the deflection) will be ignored. However, all of these details will be included in the numerical calculations in section 4. For now, we model the number density of energetic charged particles in the air shower as

$$n_{EAS}(x_o, y_o, z_o, t_o) = N_{EAS}\delta(u_x t_o - x_o)\delta(u_z t_o - z_o)\delta(y_o), \tag{11}$$

where N_{EAS} is the number of secondary charged particles in the air shower at that altitude, given by equation (9), and u_x and u_z are the components of the air shower velocity vector, $\vec{u}$. As shown in Figures 1 and 2, for convenience, the coordinate system is chosen so that the shower is in the x-z plane with $u_x > 0$.

[27] Since near shower maximum, most of the energetic charged particles in the air shower are electrons and positrons, with a typical energy of about 30 MeV, it is reasonable that these particles produce additional energetic electrons that run away at a rate u/λ, similar to the rate that the runaway electrons produce additional energetic electrons. As a result, the density of energetic seed electrons produced by the air shower is given by

$$n_s(x_o, y_o, z_o, t_o) = \frac{u}{\lambda} n_{EAS}(x_o, y_o, z_o, t_o). \tag{12}$$

[28] Using equations (7), (11) and (12), equation (8) is integrated to give

$$\begin{aligned}\rho_{re}(x', y', z', t') = {} & \frac{-euN_{EAS}}{\lambda|u_z - v_{re}|} \exp\left(\frac{1}{\lambda}\left[z' - \frac{u_z(z' - v_{re}t')}{(u_z - v_{re})}\right]\right) \\ & \cdot \delta\left(\frac{u_x(z' - v_{re}t')}{(u_z - v_{re})} - x'\right) \\ & \times \delta(y')S((u_z - v_{re})(u_z t' - z')) \\ & \cdot S((u_z - v_{re})u_z(z' - v_{re}t'))S(L - z'),\end{aligned} \tag{13}$$

where the following property of delta functions is employed when carrying out the integration:

$$\int \delta(ax - b)f(x)dx = \frac{f(b/a)}{|a|}. \tag{14}$$

In equation (13), it is assumed that $u_z \neq v_{re}$. If $u_z = v_{re}$, then integration of equation (8) gives

$$\begin{aligned}\rho_{re}(x', y', z', t') = {} & \frac{-euN_{EAS}}{\lambda|u_x|} \exp([z' - u_z x'/u_x]/\lambda)\delta(z' - v_{re}t') \\ & \cdot \delta(y')S(u_z x'/u_x)S(t' - x'/u_x)S(L - z').\end{aligned} \tag{15}$$

Note that $u_z = v_{re}$ implies that $u_x \neq 0$, since $u > v_{re}$.

[29] The current density is then

$$\vec{J}_{re}(x', y', z', t') = \vec{v}_{re}\rho_{re}. \tag{16}$$

[30] For electric field strengths that vary as $E(z)$, if the electric field can be approximated by multiple regions that each have a constant field, then the above analysis can be carried out piecewise for each region, with the runaway electrons that exit one region serving as seeds for the next. In this case,

$$\begin{aligned}n_s(x_o, y_o, z_o, t_o) = {} & \frac{u}{\lambda} n_{EAS}(x_o, y_o, z_o, t_o) + \int \frac{v_{re}}{\lambda} N_o(x_o, y_o, t'') \\ & \cdot \delta(v_{re}(t_o - t'') - z_o)dt''.\end{aligned} \tag{17}$$

In equation (17), the function N_o is the number of runaway electrons that arrive at the start of the current avalanche

region, from the end of the previous region, at the position and time (x_o, y_o, t''). This piecewise analysis is especially useful for modeling the runaway electrons that exit the avalanche region, e.g., where $E < E_{th}$. In this case, the number of runaway electrons decreases exponentially, as discussed earlier.

2.3. Low-Energy Electrons

[31] As the runaway electrons propagate, secondary electrons below the runaway threshold energy will very rapidly lose energy through ionization of the air, producing low-energy electrons at a rate given by

$$l \sim 10^4\ \mathrm{m}^{-1}(n/n_o), \tag{18}$$

the number of low-energy electron-ion pairs per meter [e.g., *Dwyer*, 2007]. The low-energy electrons will then quickly attach to oxygen and water molecules in the time τ_a, with $\tau_a \sim 10^{-8}$ sec (n_o/n). In this time, the electrons will drift in the electric field a distance, $d = v_e\tau_a$, which depends upon the electric field strength and the ambient air density, but is typically on the order of a millimeter. These low-energy electrons greatly outnumber the runaway electrons that produced them, causing a substantial contribution to the charge density, conductivity, and current.

[32] The charge density of secondary electrons is given by

$$\frac{d\rho_e}{dt} = -J_{re}l - \frac{\rho_e}{\tau_a}. \tag{19}$$

This has the general solution

$$\rho_e(x',y',z',t') = -l\int_{-\infty}^{\infty} \exp(-(t'-t'')/\tau_a) \cdot S(t'-t'')J_{re}(x',y',z',t'')dt''. \tag{20}$$

To illustrate the behavior of the low-energy electrons, consider the case of one seed particle injected at the origin at time $t_o = 0$. In this special case,

$$\vec{J}_{re}(x',y',z',t') = -e\vec{v}_{re}N_{re}(z')\delta(v_{re}t'-z')\delta(x')\delta(y'). \tag{21}$$

Inserting equation (21) into equation (20) gives the low-energy electron charge density

$$\rho_e(x',y',z',t') = -elN_{re}(z')\delta(x')\delta(y')S(v_{re}t'-z') \cdot \exp[-(v_{re}t'-z')/\lambda_e], \tag{22}$$

where $\lambda_e = v_{re}\tau_a$ is the length scale behind the avalanche front over which the low-energy electrons attach. Equation (22) shows that even though the low-energy electrons drift at a much lower speed than the runaway electrons, they form a tail behind the runaway electrons, propagating with the same speed, v_{re}.

[33] The electric current density from both the fast and slow electrons is given by

$$\vec{J}(x',y',z',t') = \vec{v}_e\rho_e(x',y',z',t') + \vec{J}_{re}, \tag{23}$$

with $\vec{v}_e$ being the drift velocity of the low-energy electrons. More generally, we could insert equations (13) and (16) into equation (20), and integrate to give the low-energy electron charge density for an arbitrary air shower trajectory. However, because λ_e is often comparable to the longitudinal diffusion of the runaway electrons and the thickness of the air shower, in order to prevent the analytical model form becoming too cumbersome, it makes more sense to include the low-energy electron tail in the numerical calculations, rather than including it in the analytical model.

[34] In the limit $\tau_a \ll \lambda/v_{re}$, the low-energy electrons have the same distribution as the runaway electrons. In this case, the contribution of the low-energy electrons to the current density is included by simply multiplying equation (16) by the factor $(1 + lv_e\tau_a)$, which is roughly a factor of 10. The low-energy electrons will be included in the following analytical calculations in this way.

3. Analytical Model of Radio Frequency Emission

[35] In this study, when calculating the RF fields, we will be working exclusively in the time domain, as opposed to the frequency domain. There are several approaches to calculating the electric and magnetic fields. In this section, we shall use the method for calculating the radiation field following *Jackson* [1975, chapters 12 and 14]. In section 4, we shall perform more complicated numerical calculations using the approach of *Uman et al.* [1975], which may be more familiar to the atmospheric electricity community.

[36] In the Lorentz gauge, the vector potential, $\vec{A}$, is related to the current density as follows [*Jackson*, 1975]

$$\vec{A}(x,y,z,t) = \frac{\mu_o}{4\pi}\int d^3\vec{x}'\int dt' \cdot \frac{\vec{J}(x',y',z',t')\delta(t'-t+R/c)S(t-t')}{R}. \tag{24}$$

[37] In the integral, the Dirac delta function, δ, and the step function, S, insure that only the part of the current density with the correct retarded time contributes to the vector potential. In this section, we are interested in the radiation field, which falls off as R^{-1}. At distances of many kilometers (for $R \gg \lambda$, where λ is the avalanche length), e.g., for thundercloud sources measured near the ground, the radiation field completely dominates over the electrostatic and induction fields (see section 4, where this approximation is verified).

[38] Because the radiation field is necessarily transverse, the scalar potential, calculated from the charge densities is not required. As a result, the radiation field can be calculated from the vector potential alone as long as care is taken

to select only the transverse component of $\vec{A}$ that falls off as $1/R$:

$$E_{rad}(x,y,z,t) = -\frac{\partial \vec{A}_{rad}}{\partial t}, \tag{25}$$

where

$$\vec{A}_{rad} = -\hat{n} \times \left(\hat{n} \times \vec{A}\right) \tag{26}$$

is the transverse component. Here $\hat{n}$ is the unit vector in the direction of the observer.

[39] The radiation magnetic field can be calculated from the electric field as follows:

$$\vec{B}_{rad} = \frac{1}{c}\hat{n} \times \vec{E}_{rad}. \tag{27}$$

[40] Consequently, in this study, the results for the radiation electric fields also apply to the radiation magnetic fields, calculated according to equation (27).

[41] We next substitute equations (13) and (16) into equation (24), including the contribution of the low-energy electrons as described at the end of section 2. For the analytical model presented here, only contributions to the current density made by electrons within the avalanche region are included. This approximation is justified because, as will be discussed further below, we are interested primarily in the rising part of the pulses, determined mostly by behavior in the avalanche region. Furthermore, because most of the current density is produced by the drifting low-energy electrons, if we assume that the electric field is zero outside the avalanche region, then relatively small currents are produced outside the avalanche region, even though the energetic electrons propagate several tens of meters into this region. In section 4, the contributions to the current density made by electrons that have exited the avalanche region are also included.

[42] To evaluate the integral, we make the assumption that R is much larger than the size of the avalanche region such that

$$R \approx R_o - \hat{n} \cdot \vec{x}', \tag{28}$$

where R_o is the distance from the observer to the origin, assumed to be located at the start of the avalanche region, and $\vec{x}'$ is the coordinate vector of the source element. In order to calculate the radiation field, the $1/R$ in equation (24) is replaced with $1/R_o$, which can be pulled out of the integral. After applying equation (28), the first delta function in equation (13) gives the relation between the x and z coordinates of the runaway electron avalanches:

$$z' = v_{re}t_{ret} + x'u_z\Omega/u_x, \tag{29}$$

where

$$\Omega = \left\{1 - \frac{v_{re}(1 - \vec{u} \cdot \hat{n}/c)}{u_z(1 - \beta\cos\theta)}\right\}, \tag{30}$$

and $\beta = v_{re}/c$. The angle, θ, is the angle to the observer with respect to the avalanche direction, $\hat{z}$. The retarded time, t_{ret}, takes into account the time for the RF signal to reach the observer at time t and is defined to be

$$t_{ret} = \frac{(t - R_o/c)}{(1 - \beta\cos\theta)}. \tag{31}$$

The resulting vector potential is then

$$\begin{aligned}\vec{A}(x,y,z,t) = {} & \frac{-e\mu_o\vec{v}_{re}uN_{EAS}(1 + lv_e\tau_a)}{4\pi\lambda|u_x|(1 - \beta\cos\theta)R_o} \\ & \times \int_{-\infty}^{\infty} \exp\left\{\frac{1}{\lambda}[(v_{re}t_{ret} + x'u_z\Omega/u_x) - (x'u_z/u_x)]\right\} \\ & \times S(u_z x'/u_x)S(L - (v_{re}t_{ret} + x'u_z\Omega/u_x)) \\ & \cdot S((v_{re}t_{ret} + x'u_z\Omega/u_x) - (x'u_z/u_x))dx'.\end{aligned} \tag{32}$$

[43] The integral in equation (32) adds the contributions of the runaway electron avalanches initiated by the air shower along its path. The first two step functions in equation (32) only allow emission from within the avalanche region to be included. The last step function only allows runaway electron avalanche positions greater than the air shower position, i.e., $z' > x'u_z/u_x$. The constant Ω includes the effects of the time delays caused by the signal propagation from the source to the observer, thereby affecting the limits of integration in equation (32).

[44] The solution to equation (32) has the form

$$\begin{aligned}\vec{A}(x,y,z,t) = {} & \frac{-e\vec{v}_{re}N_{EAS}(1 + lv_e\tau_a)}{4\pi\varepsilon_o c^2(v_{re}/u)(1 - \vec{u} \cdot \hat{n}/c)R_o} \\ & \cdot \exp\left\{\frac{1}{\lambda}[(v_{re}t_{ret} + x'u_z\Omega/u_x) - (x'u_z/u_x)]\right\}\Bigg|_{x_1}^{x_2},\end{aligned} \tag{33}$$

where the limits of integration, x_1 and x_2, are determined by the step functions in equation (33) and depend upon the signs of Ω and u_z. Note that in equation (33) and below, the permeability is replaced with the permittivity of free space. Evaluating these limits of integration for all cases gives the following solutions:

$\Omega < 0$, $u_z > 0$:

$$\begin{aligned}\vec{A}(x,y,z,t) = {} & \frac{-e\vec{v}_{re}N_{EAS}(1 + lv_e\tau_a)}{4\pi\varepsilon_o c^2(v_{re}/u)(1 - \vec{u} \cdot \hat{n}/c)R_o} \\ & \times \begin{cases} \exp(v_{re}t_{ret}/\lambda) - 1 & for\ 0 < v_{re}t_{ret} \le L \\ \exp\left(\dfrac{v_{re}t_{ret}}{\lambda\Omega} - L\dfrac{(1 - \Omega)}{\lambda\Omega}\right) - 1 & for\ L < v_{re}t_{ret} \le L(1 - \Omega) \end{cases},\end{aligned} \tag{34}$$

$\Omega = 0$, $u_z > 0$:

$$\begin{aligned}\vec{A}(x,y,z,t) = {} & \frac{-e\vec{v}_{re}N_{EAS}(1 + lv_e\tau_a)}{4\pi\varepsilon_o c^2(v_{re}/u)(1 - \vec{u} \cdot \hat{n}/c)R_o} \\ & \cdot \{\exp(v_{re}t_{ret}/\lambda) - 1\} \quad for\ 0 < v_{re}t_{ret} \le L,\end{aligned} \tag{35}$$

$\Omega > 0$, $u_z > 0$:

$$\vec{A}(x,y,z,t) = \frac{-e\vec{v}_{re}N_{EAS}(1+lv_e\tau_a)}{4\pi\varepsilon_o c^2(v_{re}/u)(1-\vec{u}\cdot\hat{n}/c)R_o} \times \begin{cases} \exp(v_{re}t_{ret}/\lambda)-1 & for \quad 0 < v_{re}t_{ret} \le L(1-\Omega) \\ \exp(v_{re}t_{ret}/\lambda) - \exp\left(\dfrac{v_{re}t_{ret}}{\lambda\Omega} - L\dfrac{(1-\Omega)}{\lambda\Omega}\right) & for \quad L(1-\Omega) < v_{re}t_{ret} \le L \end{cases}, \tag{36}$$

$\Omega > 0$, $u_z < 0$:

$$\vec{A}(x,y,z,t) = \frac{-e\vec{v}_{re}N_{EAS}(1+lv_e\tau_a)}{4\pi\varepsilon_o c^2(v_{re}/u)(1-\vec{u}\cdot\hat{n}/c)R_o} \times \begin{cases} \exp\left(\dfrac{v_{re}t_{ret}}{\lambda\Omega} - L\dfrac{(1-\Omega)}{\lambda\Omega}\right)-1 & for \quad L(1-\Omega) < v_{re}t_{ret} \le 0 \\ \exp\left(\dfrac{v_{re}t_{ret}}{\lambda\Omega} - L\dfrac{(1-\Omega)}{\lambda\Omega}\right) - \exp(v_{re}t_{ret}/\lambda) & for \quad 0 < v_{re}t_{ret} \le L \end{cases}, \tag{37}$$

and $\Omega \le 0$, $u_z < 0$: Not possible.

[45] Using equations (25) and (26), the radiation electric fields are easily found by differentiating equations (34)–(37):

$\Omega < 0$, $u_z > 0$:

$$\vec{E}_{rad}(x,y,z,t) = \frac{-\hat{n}\times(\hat{n}\times\vec{v}_{re})euN_{EAS}(1+lv_e\tau_a)}{4\pi\varepsilon_o c^2(1-\vec{u}\cdot\hat{n}/c)(1-\beta\cos\theta)\lambda R_o} \times \begin{cases} \exp(v_{re}t_{ret}/\lambda)-1 & for \quad 0 < v_{re}t_{ret} \le L \\ \dfrac{1}{\Omega}\exp\left(\dfrac{v_{re}t_{ret}}{\lambda\Omega} - L\dfrac{(1-\Omega)}{\lambda\Omega}\right)-1 & for \quad L < v_{re}t_{ret} \le L(1-\Omega) \end{cases}, \tag{38}$$

$\Omega = 0$, $u_z > 0$:

$$\vec{E}_{rad}(x,y,z,t) = \frac{-\hat{n}\times(\hat{n}\times\vec{v}_{re})euN_{EAS}(1+lv_e\tau_a)}{4\pi\varepsilon_o c^2(1-\vec{u}\cdot\hat{n}/c)(1-\beta\cos\theta)\lambda R_o}\exp(v_{re}t_{ret}/\lambda) \quad for \quad 0 < v_{re}t_{ret} \le L, \tag{39}$$

$\Omega > 0$, $u_z > 0$:

$$\vec{E}_{rad}(x,y,z,t) = \frac{-\hat{n}\times(\hat{n}\times\vec{v}_{re})euN_{EAS}(1+lv_e\tau_a)}{4\pi\varepsilon_o c^2(1-\vec{u}\cdot\hat{n}/c)(1-\beta\cos\theta)\lambda R_o} \times \begin{cases} \exp(v_{re}t_{ret}/\lambda) & for \quad 0 < v_{re}t_{ret} \le L(1-\Omega) \\ \exp(v_{re}t_{ret}/\lambda) - \dfrac{1}{\Omega}\exp\left(\dfrac{v_{re}t_{ret}}{\lambda\Omega} - L\dfrac{(1-\Omega)}{\lambda\Omega}\right) & for \quad L(1-\Omega) < v_{re}t_{ret} \le L \end{cases}, \tag{40}$$

$\Omega > 0$, $u_z < 0$:

$$\vec{E}_{rad}(x,y,z,t) = \frac{-\hat{n}\times(\hat{n}\times\vec{v}_{re})euN_{EAS}(1+lv_e\tau_a)}{4\pi\varepsilon_o c^2(1-\vec{u}\cdot\hat{n}/c)(1-\beta\cos\theta)\lambda R_o} \times \begin{cases} \dfrac{1}{\Omega}\exp\left(\dfrac{v_{re}t_{ret}}{\lambda\Omega} - L\dfrac{(1-\Omega)}{\lambda\Omega}\right) & for \quad L(1-\Omega) < v_{re}t_{ret} \le 0, \\ \dfrac{1}{\Omega}\exp\left(\dfrac{v_{re}t_{ret}}{\lambda\Omega} - L\dfrac{(1-\Omega)}{\lambda\Omega}\right) - \exp(v_{re}t_{ret}/\lambda) & for \quad 0 < v_{re}t_{ret} \le L \end{cases} \tag{41}$$

and $\Omega \le 0$, $u_z < 0$: Not possible.

[46] It is important to point out that for electric field measurements near the ground, which is usually assumed to be a good conductor, the horizontal component is very small, and the vertical component doubles. This effect is included below.

[47] As a specific example, for the case that the air shower velocity $\vec{u} = \vec{v}_{re}$, then $\Omega = 0$ and equation (39) becomes

$$\vec{E}_{rad}(x,y,z,t) = \frac{-\hat{n}\times(\hat{n}\times\vec{v}_{re})e\beta N_{EAS}(1+lv_e\tau_a)}{4\pi\varepsilon_o c(1-\beta\cos\theta)^2\lambda R_o} \cdot \exp(v_{re}t_{ret}/\lambda) \quad for \quad 0 < v_{re}t_{ret} \le L. \tag{42}$$

[48] Equation (42) is applicable to an approximately vertical air shower passing downward through an upward directed electric field, e.g., the field below the main negative charge center in a thundercloud. Note that the electric field increases exponentially with an e-folding time $\lambda(1-\beta\cos\theta)/v_{re}$.

[49] For the case that the air shower velocity $\vec{u} = -\vec{v}_{re}$, then $\Omega = 2$ and equation (41) becomes

$$\vec{E}_{rad}(x,y,z,t) = \frac{-\hat{n}\times(\hat{n}\times\vec{v}_{re})e\beta N_{EAS}(1+lv_e\tau_a)}{4\pi\varepsilon_o c\left(1-\beta^2\cos^2\theta\right)\lambda R_o} \times \begin{cases} \frac{1}{2}\exp\left(\frac{v_{re}t_{ret}}{2\lambda}+\frac{L}{2\lambda}\right) & for \quad -L < v_{re}t_{ret} \le 0. \\ \frac{1}{2}\exp\left(\frac{v_{re}t_{ret}}{2\lambda}+\frac{L}{2\lambda}\right) - \exp(v_{re}t_{ret}/\lambda) & for \quad 0 < v_{re}t_{ret} \le L \end{cases} \tag{43}$$

Equation (43) is applicable to approximately vertical air showers passing downward through a downward directed electric field, e.g., the field between the main positive and main negative charge centers in a thundercloud.

3.1. Timing

[50] In the above solutions, the air shower will strike the ground at time $R_o/u = H/[u\cos\theta_{cr}]$, where H is the altitude of the start of the avalanche region and θ_{cr} is the angle of the air shower core with respect to vertical. By determining the height of the avalanche region, e.g., utilizing a time-of-arrival technique using multiple antennas, then the relative timing of the RF pulse and the air shower can be calculated. For a colocated RF antenna and air shower array, the RF electric field is given by equations (40) and (41) for upward and downward thundercloud electric fields, respectively, and $\Omega \sim 1$. The time that the electric field will peak is then given by

$$t_{peak} \approx \frac{R_o}{c} + (L-(\Omega+1)\lambda)\frac{(1-\beta\cos\theta)}{v_{re}}, \tag{44}$$

where again, L is the length of the avalanche region. Since $u \sim c$, the air shower arrives approximately at time R_o/c. In order to measure an RF pulses L must be longer than several λ. On the other hand, relativistic feedback limits L in most cases to less than about 12λ. If we take $L = 12\lambda$, then the time interval between that the RF electric field peak and the air shower arrival is

$$\Delta t_{peak} < 10\lambda\frac{(1-\beta\cos\theta)}{v_{re}}, \tag{45}$$

independent of the altitude and distance of the source region.

[51] In section 5, we will discuss how λ can be found using the risetime of the RF pulse. The angle θ can be determined either from the air shower incidence angle if we assume a vertical (up or down) thundercloud electric field, or from multiple antennas using the distributions of RF pulse heights as shown in Figures 8 and 9 below. For instance, at 45° with respect to vertical with a 375 kV/m electric field at 5 km altitude, the RF pulse is delayed with respect to the air shower by 4×10^{-7} s for an upward thundercloud electric field, and by 2×10^{-6} s for a downward electric field. These tight constraints on the arrival times should help reduce chance coincidences between air showers and RF pulses from other sources in the thundercloud.

3.2. Comparison With Previous Work

[52] In this section we shall make a direct comparison of this work with the results of the work by *Roussel-Dupré and Gurevich* [1996] and *Tierney et al.* [2005]. To match the assumptions used by those authors as closely as possible, we consider the special case of one seed particle traveling through the avalanche region with the same velocity as the runaway electrons. We also include the low-energy electron distribution given by equation (22) and (23). The resulting current is

$$\vec{J}(x,y,z,t) = -el\vec{v}_e\exp(z/\lambda)\delta(x)\delta(y)S(v_{re}t-z)\exp[-(v_{re}t-z)/\lambda_e] - e\vec{v}_{re}\exp(z/\lambda)\delta(x)\delta(y)\delta(v_{re}t-z). \tag{46}$$

Inserting this current into equation (24), integrating, and using equations (25) and (26) to calculate the radiation electric field gives

$$\vec{E}_{rad} = \frac{-\hat{n}\times(\hat{n}\times\vec{v}_{re})e\beta}{4\pi\varepsilon_o c(1-\beta\cos\theta)^2\lambda R_o}\exp(v_{re}t_{ret}/\lambda) \cdot \left[1+\frac{lv_e\tau_a(1-\beta\cos\theta)}{(1-\beta\cos\theta)+v_{re}\tau_a/\lambda}\right]. \tag{47}$$

The peak electric field magnitude is therefore

$$E_p = \frac{ev_{re}}{R_o c\lambda}\frac{\beta\exp(\xi)\sin\theta}{4\pi\varepsilon_o(1-\beta\cos\theta)^2}\left[1+\frac{lv_e\tau_a(1-\beta\cos\theta)}{(1-\beta\cos\theta)+v_{re}\tau_a/\lambda}\right], \tag{48}$$

where ξ is the number of avalanche lengths. After translating the symbols and converting to SI units, the comparable expression from [*Roussel-Dupré and Gurevich*, 1996; *Tierney et al.*, 2005] is

$$E_p = \frac{ev_{re}}{R_o c\lambda}\frac{\beta\exp(\xi)\sin\theta}{4\pi\varepsilon_o(1-\beta\cos\theta)^2}\left[1+\frac{\langle\varepsilon_r\rangle}{34eV}\frac{v_e}{v_{re}}\frac{(1-\beta\cos\theta)}{(1-(v_e/c)\cos\theta)}\right], \tag{49}$$

which has both obvious similarities and differences. Due to the expressions in the square brackets, generally, equation (49) will overestimate the RF electric field compared to equation (48). Equations (48) and (49) will be approximately

equal in the limit $v_{re}\tau_a \gg \lambda$. However, this condition will never be satisfied for reasonable thundercloud electric fields below the conventional breakdown field. Finally, because the formula by *Roussel-Dupré and Gurevich* [1996] and *Tierney et al.* [2005] does not include the motion of the air shower, it is not easily generalized and is not applicable to the present investigation.

[53] On the observational side, *Gurevich et al.* [2004a] reported an association between fast RF pulses and energetic particles both measured at approximately the same location on a mountain. However, nearly all of their RF pulses preceded their energetic particle triggers by several tens of microseconds (backward from equation (44)). As they pointed out in their study, it is very unlikely that they were directly measuring air showers. Furthermore, how their energetic particles are related to the RF pulses has not been established. As a result, it has not known whether or not these pulses that *Gurevich et al*. reported are produced by air showers, although the duration and magnitude of the pulses are reasonably close to that predicted in this study.

4. Detailed Model

[54] In reality, the runaway electron avalanche resulting from an air shower will have a more complicated structure than that used in the simple analytical model above. To investigate the RF pulses generated by realistic air showers and runaway electron avalanches, we shall use numerical calculations to evaluate the electric fields. For these calculations the air showers are given a lateral distribution according to equation (10) and the longitudinal distribution discussed above. The modification of the air shower by the electric field is also included. The runaway electron avalanche distribution is calculated using equations (6) and (8) with the slight simplification that the lateral and longitudinal distributions are held constant with time and have their maximum values found at the end of the avalanche region. The low-energy electron component is calculated using equation (20) and equation (23) gives the current density.

[55] Past the avalanche region, the electric field is set equal to zero, and so the number of runaway electrons exponentially decreases with an e-folding length of roughly λ_{loss} = 44 m at 5 km (see equations (1)–(3) and associated discussion). Calculations were also performed for which the electric field outside the avalanche region was set to E_{th} = 142 kV/m at 5 km, and although it does modify the pulse shape after the first peak, it does not alter the rising part of the pulse, which is the part that is primarily of interest in this study.

[56] One issue that is ignored in this study are the contributions from relativistic feedback and backward propagating air shower positrons. During relativistic feedback, positrons created by pair production from the X-ray emission of the runaway electrons turn around and travel back to the start of the avalanche region, creating more runaway electron avalanches. X-rays can also Compton backscatter to the start of the avalanche region and create additional runaway electron avalanches. In addition, for upward electric field vectors, many of the positrons in the electronic part of the air shower will be turned around by the electric field and propagate back to the start of the avalanche region, where they seed additional runaway electron avalanches. These avalanches will be delayed compared to the initial avalanches created by the air shower traversing the avalanche region and so do not greatly affect the rising part of the RF pulse. However, these secondary avalanches will modify the later parts of the RF pulse, possibly producing additional pulses. Indeed, the measurement of these secondary avalanches in the RF signal could provide important information about the avalanche region and the feedback processes. Because the role of relativistic feedback is sensitive to the geometry of the avalanche region, and the backward deflection of the positrons in the air shower requires detailed Monte Carlo simulations, we leave the investigation of these aspects to future work.

[57] In the calculation of the RF pulse, we want to include contributions from the electrostatic and induction components (see below) as well as the radiation component and investigate the pulses at realistic radial distances from the source. To accomplish this, we numerically integrate the equation

$$\begin{aligned}\vec{E}(R,\theta,\varphi,t) = \frac{1}{4\pi\varepsilon_o}\iiint dV'\Bigg\{&\cos\theta\left[\frac{2}{R^3}\int_{-\infty}^{t} J(\vec{x}',t'-R/c)dt' + \frac{2}{cR^2}J(\vec{x},t-R/c)\right]\hat{n}_r \\ &+ \sin\theta\left[\frac{1}{R^3}\int_{-\infty}^{t} J(\vec{x}',t'-R/c)dt' + \frac{1}{cR^2}J(\vec{x}',t-R/c) + \frac{1}{c^2R}\frac{\partial J(\vec{x}',t-R/c)}{\partial t}\right]\hat{n}_\theta\Bigg\},\end{aligned} \tag{50}$$

which was derived by *Uman* [2001, p. 328] for the total electric field, in spherical coordinates. The terms that depend upon $1/R^3$ are called the electrostatic fields or dipole field. The terms that depend upon $1/R^2$ are called the induction field, and the term that depends upon $1/R$ is called the radiation field.

[58] To illustrate the properties of the RF emission, we shall consider a few specific cases. For the following calculations, the avalanche region will be taken to be at an altitude of 5 km, a typical height for lightning initiation for cloud-to-ground lightning. Using a higher altitude, does not change any of the basic results or the conclusions. Because the avalanche region is relatively small, for simplicity, the effect of the reduced air density at 5 km is included, but within the avalanche region the density is assumed to be approximately constant. We first consider the electric field vector pointed up (positive z is directed toward the ground as in section 3). This case corresponds to the region between the main negative and the lower positive charge centers in thunderclouds, where negative cloud-to-ground lightning is thought to initiate. The simulation used a 375 kV/m electric field strength, 310 m deep and traversed by a 10^{17} eV air shower at 30° with respect to vertical. This electric field strength has a sea level equivalent of 750 kV/m, which is $^1/_4$ the conventional breakdown field strength of 3000 kV/m. The avalanche length for this field strength is λ = 31 m at 5 km. Therefore L = 310 m corresponds to 10 avalanche lengths. The maximum avalanche multiplication is then $e^{10} = 2.2 \times 10^4$. This modest value is reasonable given the large potential

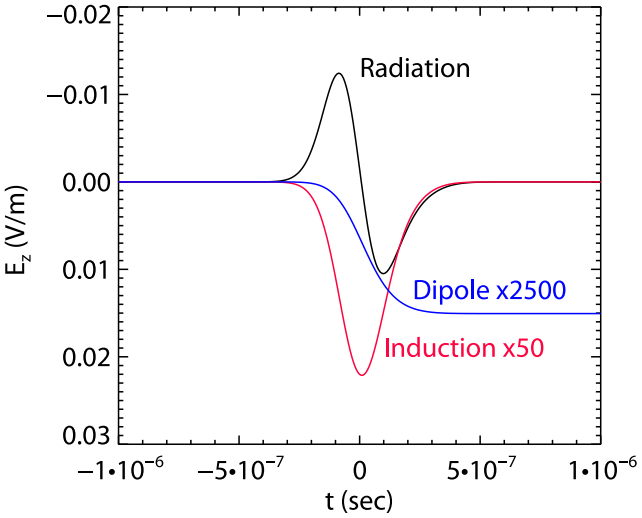

Figure 4. Pulse shape of the vertical electric field versus time as measured near the ground by an antenna located near the air shower core. The black curve is the radiation field. The red curve is the induction field multiplied by 50, and the blue curve is the electrostatic (dipole) field multiplied by 2500. The simulation used a 375-kV/m upward electric field at ~300 m deep (10 avalanche lengths), traversed by a 10^{17}-eV air shower at 30°. As can be seen, the radiation field dominates over the other components, even for relatively nearby measurements (horizontal distance = 3 km).

differences that are thought to exist within thunderclouds and is within the limit set by relativistic feedback [*Dwyer*, 2003, 2007, 2008].

[59] For several of the figures in the study, the RF field will be calculated at the location that the air shower strikes the ground, anticipating one possible experiment where the vertical RF electric field is measured at the same location as the air shower, e.g., using an array of particle detectors. Generally, the two measurements need not be made in the same location. However, apart from the practicality of having both experiments at one spot, there are two advantages to colocating them. First, the spreading of the RF pulse due to the lateral width of the air shower is minimal when the RF pulses are measured along the shower axis. Second, due to the $1/(1 - \vec{u} \cdot \hat{n}/c)$ dependence of the RF electric field (see above), the RF pulse will be largest near the position where the air shower strikes the ground. Note: due to the deflection of the electronic component of the air shower by the thundercloud electric field, the peak is shifted slightly.

[60] Figure 4 shows the vertical electric field for the radiation, induction and electrostatic components that would be measured on the ground at the same location that the air shower strikes. In Figure 4, the induction and electrostatic (dipole) components are multiplied by 50 and 2500, respectively, so that they can be viewed on the same plot. As can be seen, in this case the radiation component completely dominates, justifying the analytical approach of section 3. With the exception of measurements made along the runaway electron direction ($\theta \sim 0$), this will remain true for other geometries. Roughly, the induction term will be λ/R_o smaller than the radiation term and the electrostatic term will be λ/R_o smaller than the induction term, where λ is the avalanche length. Because the RF pulse duration is roughly equal to the avalanche length divided by the speed of light (see Figure 5), the avalanche length, λ, is approximately equal to the peak wavelength of the RF emission. Finally, we note that over much longer time periods, the drifting ions will eventually contribute to the electrostatic component.

[61] We next consider the dependence of the RF pulse shape on the electric field strength in the avalanche region. Figure 5 shows the RF pulses that would be measured on the ground as in Figure 4, except the air shower is at 45° with respect to vertical. In Figure 5, the thundercloud electric field has values of 1250 kV/m (black), 625 kV/m (red), 375 kV/m (blue), and 250 kV/m (green). In all cases, the length of the avalanche region is chosen so that there are 10 avalanche lengths. As can be seen, there is a very large change in the pulse width when going from low fields to high fields. Indeed, this change is so dramatic that simply measuring the pulse width by eye can give a reasonably good estimate of the electric field strength inside the thundercloud.

[62] To make the connection of the pulse shape and the thundercloud electric field more quantitative, we compare the result of the simple analytical model to the full numerical simulations in Figures 6 and 7. Because the rising parts of the pulses contain most of the information about the

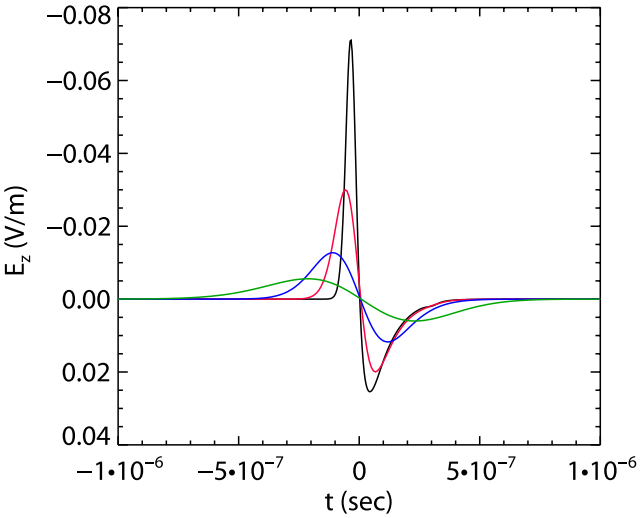

Figure 5. Pulse shape of the vertical electric field versus time as measured near the ground by an antenna located near the air shower core. The black curve is for a thundercloud electric field of 1250 kV/m, the red curve is for 625 kV/m, the blue curve is 375 kV/m, and the green curve is 250 kV/m. The high-field regions are all located at an altitude of 5 km, and the fields are directed upward. For each thundercloud field strength, the depth of the avalanche region was chosen to correspond to 10 avalanche lengths. The simulations used a 10^{17}-eV air shower at 45° with respect to vertical. As can be seen, the pulse shape measured remotely on the ground is extremely sensitive to the electric field strength inside the thundercloud. Indeed, even by eye, the approximate thundercloud electric field can be deduced.

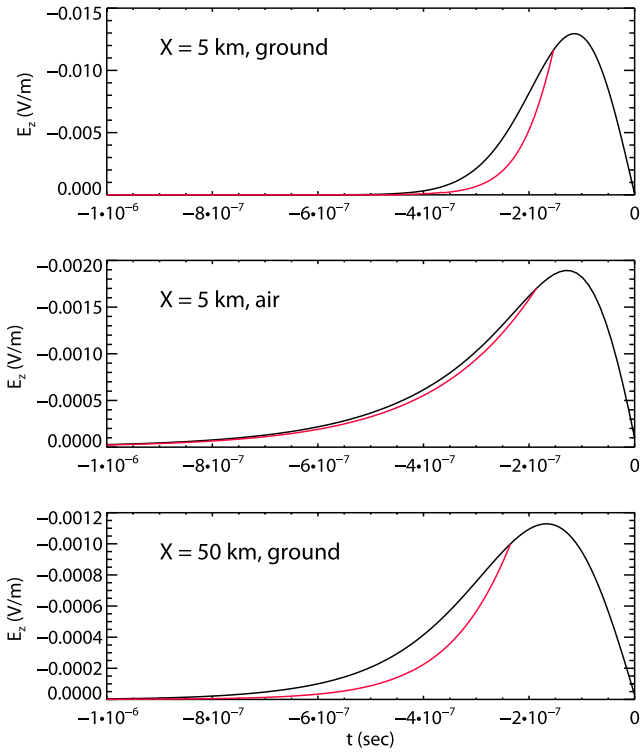

Figure 6. Pulse shape of the vertical electric field versus time as measured near the ground by an antenna located near the air shower core. In these panels, only the first half of the bipolar pulses are shown to emphasize the part of the pulses sensitive to the electric field in the avalanche region. The black curves show the total electric field pulse from numerical calculations, including a realistic air shower, diffusion of the runaway electron avalanches and low-energy electrons. The red curves are the simple analytical models that treat the air shower, runaway electron avalanche, and low-energy electrons as propagating point charges. All curves have been normalized so that the red and black curves meet at 90% of the pulse height of the black curves. The simulation used a 375-kV/m upward electric field at ~300 m deep (10 avalanche lengths), traversed by a 10^{17}-eV air shower at 45° with respect to vertical. (top) An antenna located on the ground where the air shower core strikes (horizontal distance of 5 km from runaway avalanche region). (center) The same horizontal position, but at an altitude of 10 km. (bottom) An antenna located 50 km away on the ground. The plots illustrate that the rising part of the simple analytical models match the full numerical simulation reasonably well, thus allowing very simple calculations of the thundercloud electric fields from the measured RF pulses.

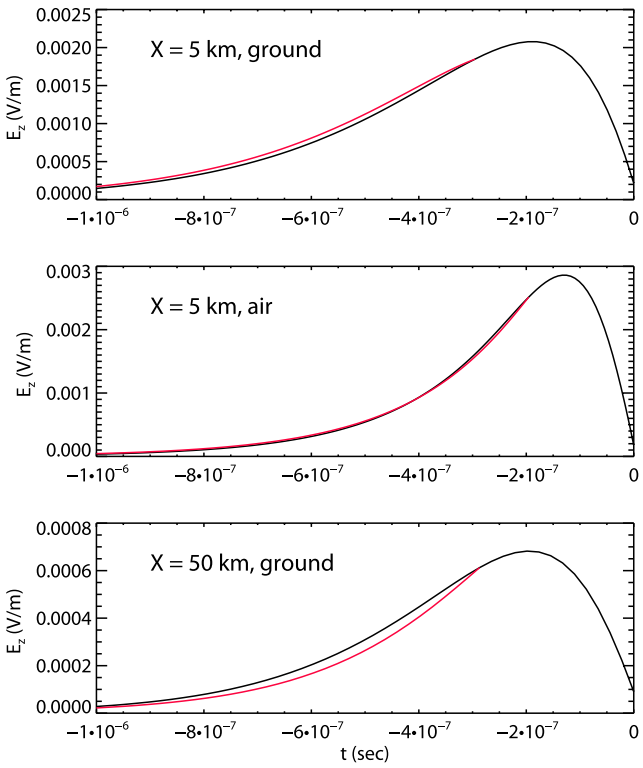

Figure 7. Same as Figure 6, except the thundercloud electric field is directed downward.

electric field in the avalanche region, we plot only the first half of the bipolar pulses. In Figure 6, the configuration is identical to that in Figure 5, except that two additional antenna locations are considered. The top panel shows the pulse located on the ground where the air shower strikes (same as Figure 5). The middle panel shows the vertical electric field that would be measured at z = 10 km above that point. This measurement might be carried out by an aircraft or a balloon, potentially located outside the thundercloud. When the location is directly above the point that the air shower strikes and the altitude is twice that of the avalanche region, then as on the ground, the effects of the lateral width of the air shower are minimal. The bottom panel shows the measurement made on the ground 50 km away in the same x direction as the shower propagates. In all three panels, the black curves are the numerical model and the red curves are the analytical models (equations (38)–(41)). Generally, the analytical model overestimates the peak RF field by about a factor of 2 compared with the more detailed numerical model. Because we are interested in the pulse shapes, the red curves are normalized so that they equal the black curves at 90% the peak value. As can be seen, although the two sets of curves do not match perfectly, they are close enough to justify one using the simpler analytical model. Correction factors that correct for the mismatch in the analytical and numerical models are presented below in Tables 1–4.

[63] Figure 7 is the same as Figure 6, except the electric field in the avalanche region is reversed. This field configuration might correspond to the field between the main positive and main negative charge centers. Again, the match

Table 1. Correction Factor in Equation (56) for an Upward Thundercloud Electric Field ($E_z > 0$) and an RF Antenna on the Ground Located at the Air Shower Strike Point

θ	$C_3^+(\theta)$
30°	1.53
45°	1.26
60°	1.08

Table 2. Correction Factor in Equation (56) for an Upward Thundercloud Electric Field ($E_z > 0$) and an Airborne RF Antenna Located Above the Air Shower Strike Point at Twice the Altitude of the Source Region

θ	$C_1(\theta)$
30°	1.0
45°	1.0
60°	1.03

between the analytical model and the full numerical solution is good.

[64] An important consideration is how large the RF pulses are, especially for more remote measurements. Figure 8 and 9 show the peak electric field versus horizontal distance for the same conditions used in Figures 6 and 7, respectively. The y axis is the value of the peak vertical electric field and the x axis is horizontal position in the direction along the shower axis. As can be seen, the distributions are peaked near the location that the air shower strikes the ground at +5 km. This is due to the relativistic motion of the air shower. A relativistic beaming due to the motion of the runaway electrons occurs near the origin. However, the vertical component of the field goes to zero at the origin as well, so the beaming due to the motion of the runaway electrons is less apparent. These patterns are fairly distinctive and it may be possible to use these patterns to identify the RF pulses from air showers and runaway electron avalanches, by employing multiple antennas, spaced several km apart. In this case, an air shower array may not be necessary. Another advantage of using multiple antennas is that the direction of the runaway electrons and hence the electric field in the avalanche region can be identified by locating the minima in the RF pulses heights (e.g., at the origin in Figures 8 and 9).

5. Electric Field at the Source

[65] Inspecting equations (38)–(41), all the time dependence in the equations is contained in either one or two exponential terms. Furthermore, Ω and θ can be determined by the air shower direction if we assume a vertical electric field. Note that the sign of the RF pulse determines the polarity of the thundercloud electric field in the avalanche region. If we choose not to assume a vertical field then an array of RF antenna on the ground can be used to determine the electric field direction as discussed above. As a result, the time variation can be used to calculate λ, which then determines the electric field strength above the avalanche threshold, E_{th}, in the avalanche region. If the air density (i.e., altitude) in the avalanche region is also known, then the runaway avalanche threshold, E_{th}, is known and the exact value of the electric field is determined. The best approach is to fit the RF pulse with the numerical simulations to determine the best fit thundercloud electric field.

Table 3. Correction Factor in Equation (56) for a Downward Thundercloud Electric Field ($E_z < 0$) and an RF Antenna on the Ground Located at the Air Shower Strike Point

θ	$C_2(\theta)$
30°	1.0
45°	1.01
60°	1.02

Table 4. Correction Factor in Equation (56) for a Downward Thundercloud Electric Field ($E_z < 0$) and an Airborne RF Antenna Located Above the Air Shower Strike Point at Twice the Altitude of the Source Region

θ	$C_3^-(\theta)$
30°	0.98
45°	0.99
60°	1.0

A slightly simpler approach is to fit the full analytical models. In this section, we shall present an even simpler approximation that allows a quick and easy calculation of the thundercloud electric field based upon the rising part of the RF pulse.

[66] In equations (38)–(41), if the e-folding times of the two exponential functions are not too similar, then, for times earlier than when the electric field peaks, the exponential function with the longest e-folding time will dominate. Let us consider three possibilities: $\Omega < 1$ and $\Omega > 1$, and $\Omega \sim 1$. In the first case, the electric field has the approximate e-folding time $\lambda(1 - \beta \cos\theta)/v_{re}$. For $\Omega > 1$, the electric field has the approximate e-folding time $\Omega\lambda(1 - \beta \cos\theta)/v_{re}$. Finally, for the $\Omega \sim 1$ case, the time dependence can be approximated by the form

$$E_{rad} \propto \frac{(\Omega - 1)}{\Omega}\left(\frac{v_{re}t_{ret} - L}{\lambda\Omega} + 1\right)\exp(v_{re}t_{ret}/\lambda). \qquad (51)$$

Differentiating gives

$$\frac{dE_{rad}}{dt} \propto \frac{(\Omega - 1)}{\Omega}\left(t - t_{peak}\right)\exp(v_{re}t_{ret}/\lambda), \qquad (52)$$

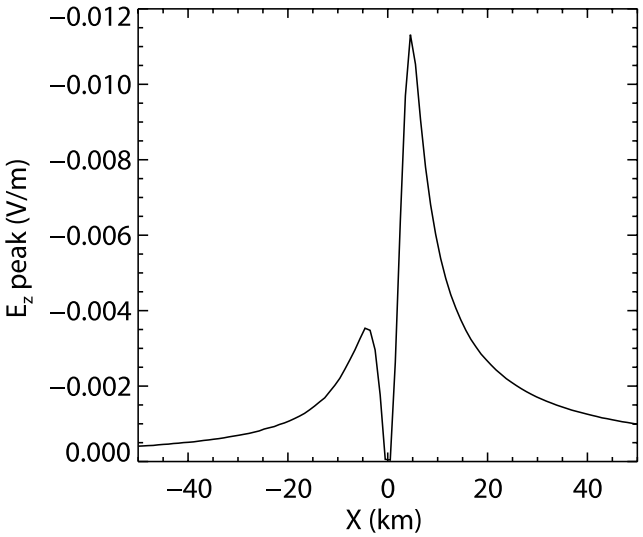

Figure 8. Peak vertical electric field magnitude versus horizontal distance. The simulation used a 375-kV/m upward electric field at ~300 m deep (10 avalanche lengths), traversed by a 10^{17}-eV air shower at 45° with respect to vertical. The air shower core strikes the ground at +5 km. The off axis maximum near +5 km is due to the relativistic motion of the air shower. The relativistic motion of the runaway electrons also contributes to an enhancement near the origin.

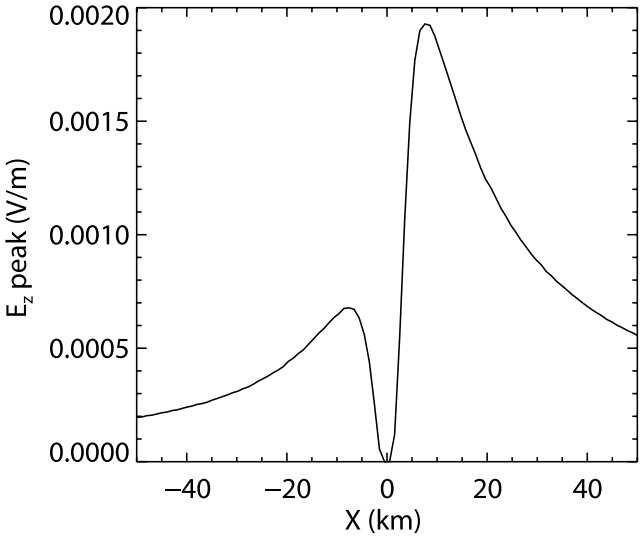

Figure 9. Same as Figure 8, except the thundercloud electric field is directed downward.

where t_{peak} is the time that the RF electric field pulse is observed to reach its maximum and is given by equation (44). Equations (31) and (52) then give the relationship

$$\frac{dE_{rad}/dt}{(t-t_{peak})\int_{-\infty}^{t}\frac{dE_{rad}/dt}{(t''-t_{peak})}dt''}=\frac{v_{re}}{\lambda}\frac{1}{(1-\beta\cos\theta)}. \quad (53)$$

[67] Similarly, for the $\Omega < 1$ and $\Omega > 1$ cases, we have

$$\frac{1}{E_{rad}}\frac{dE_{rad}}{dt}=\frac{E_{rad}}{\int_{-\infty}^{t}E_{rad}dt''}=\begin{cases}\frac{v_{re}}{\lambda}\frac{1}{(1-\beta\cos\theta)} & \Omega<1\\ \frac{v_{re}}{\lambda\Omega}\frac{1}{(1-\beta\cos\theta)} & \Omega>1\end{cases}. \quad (54)$$

As an example, for the $\Omega < 1$ case, using equation (54) and equations (2) and (3) for λ, we can solve for the thundercloud electric field inside the avalanche region, e.g., the static or slowly varying thundercloud electric field:

$$E=\frac{7.3\times10^{6}\mathrm{V}(1-\beta\cos\theta)}{\beta c}\frac{1}{E_{rad}}\frac{dE_{rad}}{dt}+E_o, \quad (55)$$

where $\beta = 0.89$ and $E_o = 2.76 \times 10^5$ V/m (n/n_o).

[68] When comparing with the numerical calculations, it is found that the integral form in equation (54) often gives better results. Combining this with equation (53), we can write the general expression for the thundercloud electric field in terms of the rising part of the measured RF pulses:

[69] Here the functions $C_n(\theta)$ are correction factors, on the order 1, that correct for the errors associated with using the analytical solutions (see Figures 6 and 7). These factors, which depend only the viewing angle and not the electric field are found by applying equation (56) to the numerically calculated RF pulses. Several examples of these functions are presented in Tables 1–4.

[70] Although the analytical model was derived for a uniform electric field in the avalanche region, for the case that the RF electric field is measured above the point where the air shower strikes the ground (e.g., at twice the altitude of the source region), equation (56) works remarkably well for spatially varying electric fields. This is illustrated in Figures 10 and 11, which shows the electrostatic fields inside the thundercloud at 5 km altitude. In Figures 10 and 11, two cases are shown: a uniform electric field and a uniform electric field with a high-field "hot spot" where lightning initiation may occur. The hot spot is modeled as a Gaussian perturbation. The input field for the latter case is plotted in solid black. The blue and red curves are the calculated electric field using equation (56) for the two cases based upon remote airborne measurements. As can be seen, the remote measurements accurately reproduce the electric field inside the thundercloud. Furthermore, a relatively compact high-field region, just a few tens of meters across can be measured with this technique. The measurement of such localized high-field regions would help address the lightning initiation problem, since it has been theorized that lightning is initiated in small high-field pockets. Finding and measuring such pockets otherwise would be very difficult.

[71] For RF pulses measured on the ground, few spatial details are transmitted in the RF pulses. Instead, the pulses give information about the average electric field inside the avalanche region. We have performed simulations with various electric field shapes to verify that this is indeed the case. In Figures 12–14, we plot the average electric field calculated using equation (56), plotted against the electric field used in the full numerical calculation. As can be seen, the remotely measured electric field faithfully gives the correct average electric field over a wide range of thundercloud electric field strengths. In other words, only a small correction to the overall normalization is required to give good agreement between the simple model and the simulated data. In Figure 14, we present the measurements of the electric field using remote ground based measurements, 50 km from the thundercloud. In these cases, no information about the air shower direction is assumed. As can be seen, the individual measurements have a systematic error, but the average of the two measurements provides a good determination of the thundercloud electric field.

$$E=\begin{cases}\frac{7.3\times10^{6}\,\mathrm{V}(1-\beta\cos\theta)C_1(\theta)}{\beta c}\frac{E_{rad}}{\int_{-\infty}^{t}E_{rad}dt''}+E_o & \Omega<1\\ \frac{7.3\times10^{6}\,\mathrm{V}(1-\beta\cos\theta)C_2(\theta)\Omega}{\beta c}\frac{E_{rad}}{\int_{-\infty}^{t}E_{rad}dt''}+E_o & \Omega>1\\ \frac{7.3\times10^{6}\,\mathrm{V}(1-\beta\cos\theta)C_3^{\pm}(\theta)}{\beta c}\frac{dE_{rad}/dt}{(t-t_{peak})\int_{-\infty}^{t}\frac{dE_{rad}/dt}{(t''-t_{peak})}dt''}+E_o & \Omega\approx1\end{cases}. \quad (56)$$

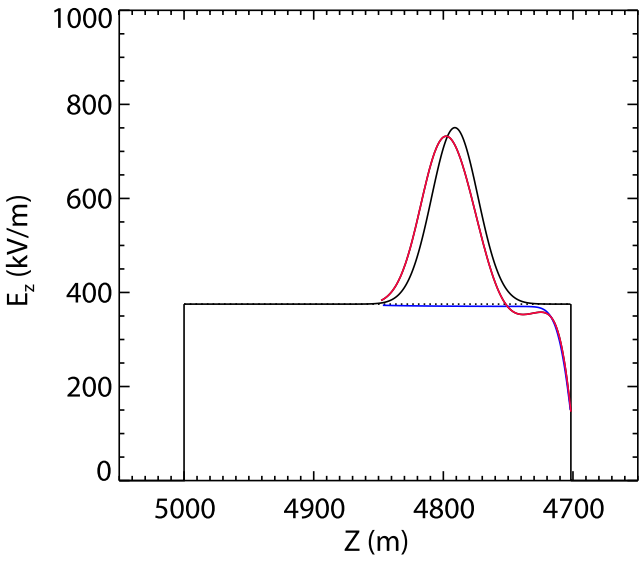

Figure 10. The thundercloud electric field that would be measured remotely along with the actual electric field. Two cases are shown: the blue curve is for a uniform electric field with strength of 375 kV/m. The red curve is for the same field but with a Gaussian enhancement (shown in black), corresponding to a small pocket with a very high field inside the thundercloud. The antenna is located directly above where the air shower core strikes the ground at an altitude of 10 km. The simulation used a 5×10^{17} eV air shower at 30°. The high-field regions are located at an altitude of 5 km and have depths corresponding to 12 avalanche lengths. As can be seen, with this technique, it should be possible to remotely (>5 km away) measure pockets with high fields measuring just a few tens of meters in depth.

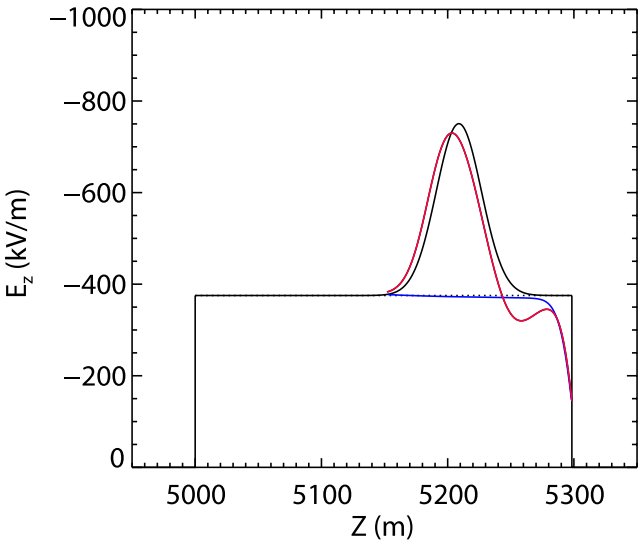

Figure 11. Same as Figure 10, except the thundercloud electric field is directed downward.

[72] We also plot in Figures 12–14 the minimum cosmic ray energies need to produce measurable RF pulses. Here it is assumed that an RF pulse greater than 1 mV/m can be measured. These numbers along with the known flux of high-energy cosmic rays gives an estimate of the frequency of measurable RF pulses that are produced in a given avalanche region. This will be discussed more below.

6. Discussion

[73] In this study, we have developed new analytical and numerical models for describing RF pulses produced by cosmic ray extensive air showers passing through runaway electron avalanche regions with arbitrary angles of inclination. We used these models to describe a new technique for remotely measuring electric fields inside or near thunderclouds. Specifically, we have shown that the shape of the RF pulses measured at large distances on or above the ground can be used to infer the value of the static (DC) or slowly varies electric field in the source region.

[74] Because the RF signal sizes are relatively small, it may be a challenge to measure and identify the pulses produced by the air shower/runaway electron avalanches. For initial studies at least, we suggest using an air shower array in conjunction with several electric field and/or magnetic field antennas. Coincidences between air showers

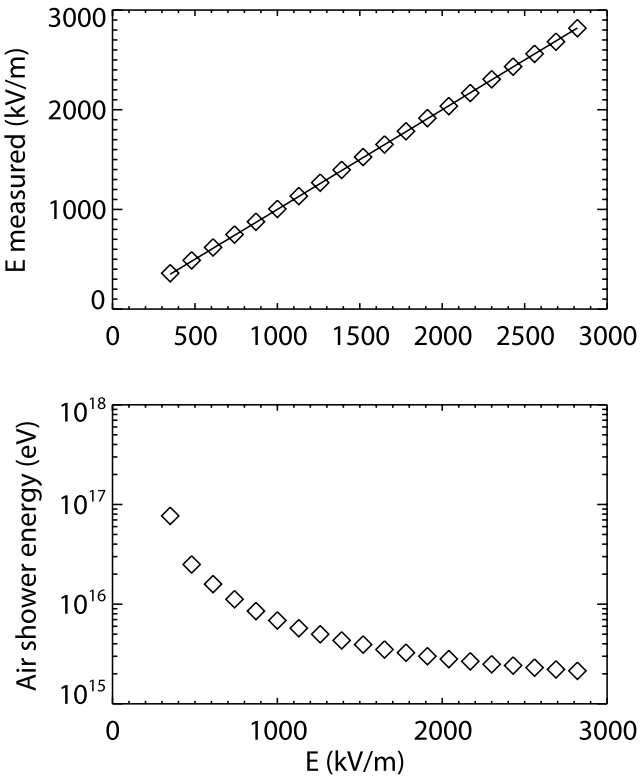

Figure 12. (top) The average thundercloud electric field that would be measured remotely versus the actual average electric field. The solid line shows unit slope. The simulation used air showers incident at 45° with the antenna located on the ground where the core strikes. The thundercloud electric fields are all directed upward, and 10 avalanche lengths were used. The energy of the air shower for each electric field strength was assumed to be large enough so that the RF pulse could be well measured down to 10% of its peak value. (bottom) The minimum air shower energy required to produce measurable (>1 mV/m) RF pulses on the ground.

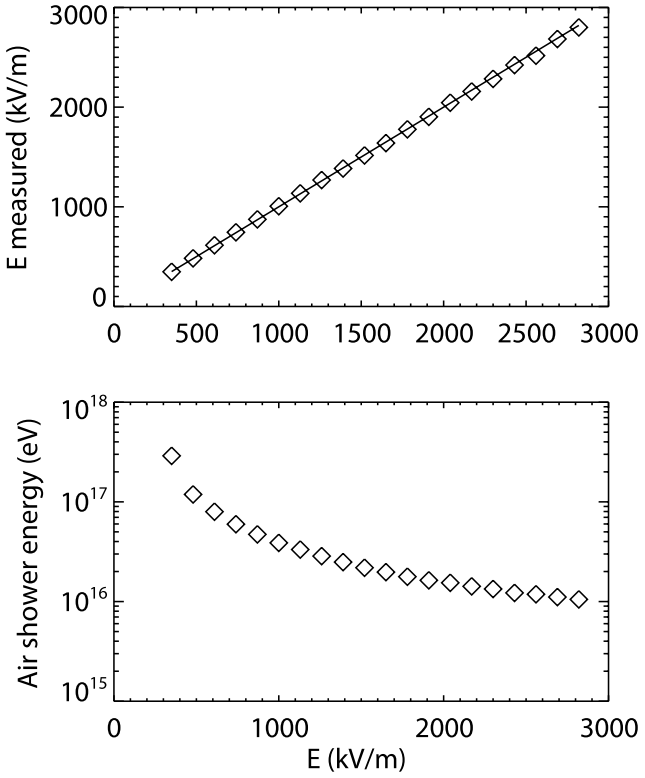

Figure 13. Same as Figure 12, except the thundercloud electric field is directed downward.

measured by the array and RF pulses measured by the antennas could then be searched for and properties of these RF pulses could be investigated. Ultimately, it would be ideal to have a large array of antennas distributed over many km that would be able to identify the correct RF pulses without the use of an air shower array, thus increasing the number of events and hence the number of remote electric field measurements. The pulses predicted in this study have several features that may allow them to be distinguished from other pulses radiated from the thundercloud. For instance, the pulses due to air shower/runaway electron avalanches are fairly short with widths ranging from 0.1–1 microsecond, and exhibit relativistic beaming, which enhances the pulse in the direction of the runaway electron avalanche and the air shower.

[75] An interesting question is whether RF pulses produced by air shower/runaway electron avalanches can account for narrow bipolar pulses (NBPs), as has been suggested by others [*Gurevich and Zybin*, 2004; *Gurevich et al.*, 2004b]. Narrow bipolar pulses are large (~1–10 V/m at 100 km) RF pulses with risetimes typically on the order of 1 microsecond [*Rakov and Uman*, 2003]. Using the above results, these facts predict an electric field at a 5 km source altitude of ~170,000 V/m for NBPs, which is a reasonable thundercloud electric field. However, the pulse heights of the NBPs are very large and, assuming an avalanche multiplication factor of 10^5, near the maximum value allowed by relativistic feedback, an air shower energy of at least 10^{20} eV would be required. In summary, either the avalanche multiplication limit set by feedback [*Dwyer*, 2003, 2007, 2008] must be somehow circumvented, or ultrahigh-energy air showers that are some of the largest and rarest ever recorded are required. If air showers are indeed associated with NBPs, another problem is that for every NBP measured in the 1–10 V/m range, there should be approximately 100 pulses in the 0.1–1 V/m range, due to the rapidly increasing flux of cosmic rays with decreasing energy. Since these smaller pulses have not been reported as part of the NBPs population, there would have to be a large observational bias in favor of the largest pulses. Consequently, it remains to be seen if NBPs have anything to do with the mechanism described in this study.

[76] One important issue to consider is the flux of air showers with sufficient energy to produce measurable RF pulses. The integral flux of air showers in the range 10^{10}–10^{20} eV (assuming an approximately isotropic arrival distribution from above) is approximately

$$I(>\mathcal{E}_{CR}) = 3\times10^{4}\mathcal{E}_{CR}^{-1.7}\ \mathrm{m^{-2}\,s^{-1}} \quad 10\,\mathrm{GeV} < \mathcal{E}_{CR} < 3\times10^{6}\,\mathrm{GeV}$$
$$I(>\mathcal{E}_{CR}) = 4\times10^{7}\mathcal{E}_{CR}^{-2.1}\ \mathrm{m^{-2}\,s^{-1}} \quad \mathcal{E}_{CR} > 3\times10^{6}\,\mathrm{GeV}, \tag{57}$$

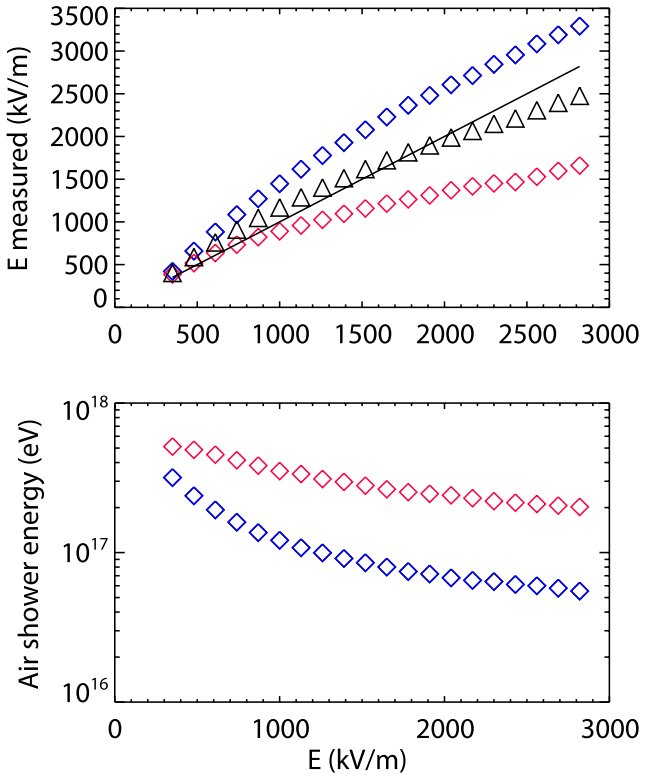

Figure 14. Same as Figure 13, except the antennas are located at horizontal distances of 50 km. The air shower is still incident at 45° with respect to vertical and strikes the ground at a horizontal distance of 5 km. The blue diamonds are for the case when air showers are traveling in the direction toward the antenna, and the red diamonds are when air showers are traveling in the opposite direction, away from the antenna. The black triangles are the average of the two. As a result, even if no information about the air shower is available, two remote RF measurements can be used to infer the thundercloud electric field. (bottom) The minimum air shower energy required to produce measurable (>1 mV/m) RF pulses on the ground.

where $\mathcal{E}_{CR}$ is the energy of the cosmic ray primary particle in GeV [*Berezinskii et al.*, 1990, p. 34]. For the cases discussed above, assuming that the width of the avalanche region is about twice its length, then an air shower with energy above 10^{17} eV would pass through the avalanche region and producing an RF pulse about once every hour, i.e., approximately once per thundercloud cell. On the other hand, as seen in Figures 12–14, air showers with energies around 10^{16} eV will still produce measurable pulses. In contrast, the rate of such air showers is once per minute, allowing the charging process to potentially be measured. It is possible that such measurements may provide information about the likelihood of lightning to initiate and may provide a warning about ripe conditions for lightning even before the first lightning flash occurs. If, on the other hand, no RF pulses with the properties presented in this work, are observed then this would seriously challenge runaway breakdown models of lightning initiation and would indicate that thunderclouds rarely reach electric fields in exceeding 1/10 the conventional breakdown field.

[77] On a related topic, it is possible that terrestrial gamma ray flashes (TGFs) are sometimes produced at source altitudes lower than 15 km and hence are not detected by spacecraft such as RHESSI or on the ground [*Smith et al.*, 2005; *Dwyer and Smith*, 2005]. However, the technique described in this study could help identify regions with large avalanche multiplication factors that may be producing TGFs that would otherwise be difficult to detect. *Dwyer* [2008] suggested the positron and X-ray (relativistic) feedback mechanism may play an important role in TGFs. Interestingly, a region experiencing large amounts of feedback should produce multiple RF pulses separated by a few microseconds when an air shower passes through it.

[78] Finally, remaining challenges will be to take into account the finite conductivity of the ground and making precise measurements of the electric and/or magnetic radiations field over the timescales of 10^{-8}–10^{-5} seconds, corresponding to the highest and lowest thundercloud electric fields likely to be measured. Specifically, the lower the magnitude of the radiation field that can be measured, the more successful this technique will be, since a more detailed mapping of the electric field with better spatial and temporal resolution would then be possible. The success of this technique will clearly depend upon the relative sizes of the signals to the noise, the latter of which will obviously limit the ability to reconstruct the thundercloud electric field from the RF measurements. Because the characteristics of the noise will depend upon both the details of the measurement system used and the environment, we have not attempted to model the impact of the noise in this study. We do acknowledge that there most likely will exist technical challenges in making these observations. However, if this technique is successful, it should be possible to remotely observe very small pockets with large electric fields within thunderclouds. Such small regions of large electric fields have long been theorized to exist in order to explain lightning initiation, but have never been observed due to the difficulty in making in situ measurements.

[79] **Acknowledgments.** We thank Ningyu Liu, Ziad Saleh, Eric Cramer, Meagan Schaal, Linnea Dwyer, and Burcu Kosar for their assistance with this study. This work was supported by NSF grant ATM 0607885 and DARPA grant HR0011-08-1-0088.

References

Berezinskii, V. S., et al. (1990), *Astrophysics of Cosmic Rays*, 34 pp., North Holland, Netherlands.

Buitink, S., et al. (2007), Amplified radio emission from cosmic ray air showers in thunderstorms, *Astron. Astrophys.*, *467*, 385–394.

Coleman, L. M., and J. R. Dwyer (2006), The propagation speed of runaway electron avalanches, *Geophys. Res. Lett.*, *33*, L11810, doi:10.1029/2006GL025863.

Dwyer, J. R. (2003), A fundamental limit on electric fields in air, *Geophys. Res. Lett.*, *30*(20), 2055, doi:10.1029/2003GL017781.

Dwyer, J. R. (2004), Implications of X-ray emission from lightning, *Geophys. Res. Lett.*, *31*, L12102, doi:10.1029/2004GL019795.

Dwyer, J. R. (2005), The initiation of lightning by runaway air breakdown, *Geophys. Res. Lett.*, *32*, L20808, doi:10.1029/2005GL023975.

Dwyer, J. R. (2007), Relativistic breakdown in planetary atmospheres, *Phys. Plasmas*, *14*(4), 042901, doi:10.1063/1.2709652.

Dwyer, J. R. (2008), Source mechanisms of terrestrial gamma-ray flashes, *J. Geophys. Res.*, *113*, D10103, doi:10.1029/2007JD009248.

Dwyer, J. R., and D. M. Smith (2005), A comparison between Monte Carlo simulations of runaway breakdown and terrestrial gamma-ray flash observations, *Geophys. Res. Lett.*, *32*, L22804, doi:10.1029/2005GL023848.

Gaisser, T. (1990), *Cosmic Rays and Particle Physics*, pp. 226, 240, Cambridge Univ. Press, Cambridge.

Gurevich, A. V., and K. P. Zybin (2001), Runaway breakdown and electric discharges in thunderstorms, *Phys. Usp.*, *44*, 1119–1140.

Gurevich, A. V., and K. P. Zybin (2004), High energy cosmic ray particles and the most powerful discharges in thunderstorm atmosphere, *Phys. Lett. A*, *329*(4–5), 341–347.

Gurevich, A. V., G. M. Milikh, and R. Roussel-Dupré (1992), Runaway electron mechanism of air breakdown and preconditioning during a thunderstorm, *Phys. Lett. A*, *165*, 463–468.

Gurevich, A. V., K. P. Zybin, and R. A. Roussel-Dupré (1999), Lightning initiation by simultaneous effect of runaway breakdown and cosmic ray showers, *Phys. Lett. A*, *254*, 79–87.

Gurevich, A. V., L. M. Duncan, Yu. V. Medvedev, and K. P. Zybin (2002), Radio emission due to simultaneous effect of runaway breakdown and extensive atmospheric showers, *Phys. Lett. A*, *301*, 320–326.

Gurevich, A. V., et al. (2004a), Experimental evidence of giant electron-gamma bursts generated by extensive atmospheric showers in thunderclouds, *Phys. Lett. A*, *325*, 389–402.

Gurevich, A. V., Yu. V. Medvedev, and K. P. Zybin (2004b), New type discharge generated in thunderclouds by joint action of runaway breakdown and extensive atmospheric shower, *Phys. Lett. A*, *329*, 348–361.

Gurevich, A. V., K. P. Zybin, and Yu. V. Medvedev (2006), Amplification and nonlinear modification of runaway breakdown, *Phys. Lett. A*, *349*, 331–339.

Huege, T., and H. Falcke (2005), Radio emission from cosmic ray air showers: Simulation results and parameterization, *Astropart. Phys.*, *24*, 116–136.

Jackson, J. D. (1975), *Classical Electrodynamics*, 2nd ed., chaps. 13 and 15, John Wiley, New York.

Jelley, J. V., J. H. Fruin, N. A. Porter, T. C. Weekes, F. G. Smith, and R. A. Porter (1965), Radio pulses from extensive cosmic-ray air showers, *Nature*, *205*, 327.

Kahn, F. D., and I. Lerche (1966), Radiation from cosmic ray air showers, *R. Soc. Lond. Proc. Ser. A*, *289*, 206.

MacGorman, D. R., and W. D. Rust (1998), *The Electrical Nature of Storms*, Oxford Univ. Press, New York.

Marshall, T. C., et al. (2005), Observed electric fields associated with lightning initiation, *Geophys. Res. Lett.*, *32*, L03813, doi:10.1029/2004GL021802.

Rakov, V. A., and M. A. Uman (2003), *Lightning Physics and Effects*, pp. 82–84, Cambridge Univ. Press, New York.

Roussel-Dupré, R., and A. V. Gurevich (1996), On runaway breakdown and upward propagating discharges, *J. Geophys. Res.*, *101*(A2), 2297–2312.

Smith, D. M., L. I. Lopez, R. P. Lin, and C. P. Barrington-Leigh (2005), Terrestrial gamma-ray flashes observed up to 20 MeV, *Science*, *307*, 1085–1088.

Solomon, R., V. Schroeder, and M. B. Baker (2001), Lightning initiation—Conventional and runaway-breakdown hypothesis, *Q. J. R. Meteorol. Soc.*, *127*, 2683–2704.

Tierney, H. E., R. A. Roussel-Dupré, E. M. D. Symbalisty, and W. H. Beasley (2005), Radio frequency emissions from a runaway electron

avalanche model compared with intense, transient signals from thunderstorms, *J. Geophys. Res.*, *110*, D12109, doi:10.1029/2004JD005381.
Tompkins, D. R., Jr. (1974), Thundercloud radio emission form cosmic-ray shower ionization electrons, *Phys. Rev. D*, *10*, 136–145.
Uman, M. A. (2001), *The Lightning Discharge*, 328 pp., Dover Publ., Mineola, New York.
Uman, M. A., D. K. McLain, and E. P. Krider (1975), The electromagnetic radiation from a finite antenna, *Am. J. Phys.*, *43*, 33–38.

J. R. Dwyer and H. K. Rassoul, Department of Physics and Space Sciences, Florida Institute of Technology, 150 West University Boulevard, Melbourne, FL 32901, USA. (jdwyer@fit.edu)
M. A. Uman, Department of Electrical and Computer Engineering, University of Florida, 311 Larsen Hall, P.O. Box 116200, Gainesville, FL 32611-6200, USA.